Research article

Bioactive and antimicrobial macro-/micro-nanoporous selective laser melted Ti–6Al–4V alloy for biomedical applications

Archana Rajendran [a,b], Deepak K. Pattanayak [a,b,*]

[a] *CSIR-Central Electrochemical Research Institute, Karaikudi, Tamil Nadu, 630006, India*
[b] *Academy of Scientific and Innovative Research (AcSIR), Ghaziabad, 201002, India*

ARTICLE INFO

ABSTRACT

Metal Additive Manufacturing (AM) technology is an emerging technology in biomedical field due to its unique ability to manufacture customized implants [Patients-specific Implants (PSIs)] replicating the complex bone structure from the relevant metal powders. PSIs could be developed through any AM technology, but the ultimate challenge lies in integrating the metallic implant with the living bone. Considering this aspect, in the present study, Ti alloy (Ti–6Al–4V) powder has been used to fabricate scaffolds of channel type macropores with 0–60% porosity using selective laser melting (SLM) and subsequent post-treatments paving way for surface microporosities. Surface chemical and subsequent heat treatments were carried out on thus developed Ti alloy scaffolds to improve its bioactivity, antibacterial activity and osteoblastic cell compatibility. NaOH and subsequent $Ca(NO_3)_2$/ $AgNO_3$ treatment induced the formation of a nanoporous network structure decorated with Ca–Ag ions. Ag nanoparticles covering the entire scaffold provided antibacterial activity and the presence of Ca^{2+} ions with anatase TiO_2 layer further improved the bioactivity and osteoblastic cell compatibility of the scaffold. Therefore, SLM technology combined with heat treatment and surface modification could be effectively utilized to create macro-micro-nano structure scaffolds of Ti alloy that are bioactive, antibacterial, and cytocompatible.

1. Introduction

In orthopaedics as well as dentistry, metallic biomaterials are widely used for hard tissue replacements to treat or replace damaged tissues or organs [1]. In recent years, Ti metal and Ti alloys are gaining more popularity as metallic biomaterials to replace fractured and diseased bones in the human body [1, 2]. A major limitation of the Ti metal and Ti alloy based implants is the bone resorption due to stress shielding, weak bone-bonding ability and the lack of strong integration at the implant-tissue interface [3]. However, when compared to dense metallic implants, a metal with adequate porosity can significantly improve bone integration thus providing suitable bonding strength or stable interlocking at the metal-bone interface. Also, these pores provide a pathway for cells to proliferate, differentiate and therefore the design of the scaffold will determine the final structure of the bone being formed.

Developing patient-specific implants with complicated shape, porosity and mechanical strength similar to fractured bones is an uphill task for a biomedical engineer [4]. So far, conventional manufacturing processes such as machining, grinding, forging, etc. were commonly being used to develop metallic implants [5]. Whereas, most of these

processes not only consume longer man-hours they also result in higher wastage of materials. Also, developing a porous metallic implant with different pore sizes and pore geometries mimicking the living bone is extremely challenging. Of late, a variety of additive manufacturing technologies have emerged to meet these challenges, including selective laser sintering, selective laser melting, electron beam melting and laser engineered net shaping etc. In these AM processes, metallic implants are constructed layer by layer, bottom to top, using CAD/CAM design data. Moreover, these AM technologies facilitate one-step fabrication of complex 3D parts which is difficult by any other conventional manufacturing techniques. Another major advantage of this AM technology is to directly develop medical devices from the computer tomography (CT) data of the fractured/defective bones received from the surgeon [6, 7, 8, 9].

Even though Ti metal and Ti alloys are medically approved implant materials, it takes longer time for the new bone to grow with strong adhesion to their surfaces inside human body. As a result, fibrous tissues grow often at the interface of implant and living bone thereby interfering new bone formation process on implant surface. To overcome this issue, scientists, medical practitioners, and engineers have been toiling hard over the years to develop implantable bioactive metallic devices that can

---

integrate and form new bones on their surfaces when implanted in the human body [10, 11, 12, 13]. Researchers have reported various calcium phosphate-based ceramic coatings that have been used to improve the bioactivity of Ti metal and its alloys thereby providing a suitable platform for the bone tissues to initially adhere and grow on its surface and then proliferate to develop new bone eventually transforming into matured bone in due course. Despite high success rate of this technique in clinical trials, it has many shortfalls such as ceramic-metal interfacial bonding, uniformity in coating etc. [10, 14, 15] All these coating based surface modification methods could be technically applied on solid Ti metal/Ti alloy implants. However, it becomes a challenge while developing porous bone scaffold with complicated internal geometry. Thus, a new surface modification approach is needed to improve the bioactivity of medical devices which should ensure uniform application even in the intricate parts of the porous scaffolds.

Further, bacterial infections pose a major threat in Ti metal-based implants, if proper sterilisation is not carried out prior to surgery [16, 17]. Even though, these infections could be controlled to an extent through antibiotics, the emergence of antibiotic-resistant strains like MRSA has reduced their efficacy [18] Thus, the need arises for a strong antimicrobial/antibacterial agent to prevent the bacterial adhesion during the early stage itself and to withstand the high temperature processing conditions of Ti metal as well [19].

Surface modification by chemical solution treatment is an effective way to provide a uniform bioactive surface over Ti metal and its alloys. Alkali-heat, alkali-acid-heat, acid-alkali-heat, mixed-acid-heat and H_2O_2 treatment are the most commonly used chemical surface modification methods to develop bioactive Ti metal and its alloys surfaces [20, 21, 22, 23, 24, 25, 26, 27, 28, 29]. Among these, alkali-heat treatment is the most common and cost-effective as it induces faster bone-bonding ability, both *in vitro* and *in vivo.* [30, 31, 32, 33, 34] However, cytotoxicity caused by the Na^+ ion release from the alkali-heat treated Ti metal/Ti alloy surface can affect the surrounding cells. To address this, in our previous study, the Na^+ ions in the alkali-heat treated Ti metal was successfully replaced by Ca^{2+} ions to improve bioactivity and attract more adhesion of bone cells on the implant surface [33]. However, the results showed that the decoration of Ca^{2+} ions retarded the apatite-forming ability of NaOH treated Ti metal in simulated body fluid (SBF). This was substantiated by the decrease in Ca^{2+} ions release and the crystalline nature of TiO_2 formed during alkali-Ca-heat treatment. Also, when alkali-Ca-heat treatment was performed, the sodium titanate formed during alkali-heat treatment got converted to calcium titanate and rutile TiO_2 [33]. In another study, we demonstrated that these Na^+ ions could be easily replaced by Ag^+ ions forming an anatase TiO_2 on the Ti metal surface. This Ag^+ ion addition not only favoured the formation of bone-like apatite in SBF but also attributed to the excellent antibacterial activity of Ti metal [32]. A detailed osteoblastic cell compatibility study of silver-incorporated Ti metal showed good adhesion, proliferation and osteogenic differentiation of human gMSCs [32].

Based on the above cited literatures, it is clearly evident that additive manufacturing will be the much sought-after future technology for developing customised implants with complicated internal geometry mimicking the patient's bone defect. However, understanding on processing of minimum pore size and pore dimension accuracy in SLM technique is an essential requirement for developing porous bone implants. Further, complementing beneficial properties such as biocompatibility, enhanced bioactivity and antibacterial activity to the SLM based Ti–6Al–4V scaffold has not been highlighted enough in the literature. Here, we have designed Ti–6Al–4V scaffold from its corresponding alloy powder by SLM technique, wherein antibacterial activity coupled with bioactivity and osteoblastic cell compatibility is attempted by co-decorating Ca^{2+} as well as Ag^+ ions using chemical treatment method. Macroporous scaffolds of varying porosities and pore morphology were attempted using the SLM process and a bioactive micro/nano-porous structure was formed on the scaffolds via chemical treatment method. An extensive investigation was conducted on the effect of Ca or Ag or Ca–Ag co-decoration on the bioactivity of the scaffolds. Meanwhile, the Ca–Ag concentration on the Ti alloy was further optimised for better antibacterial activity without causing any cytotoxicity towards osteoblast-like cells.

2. Materials and methods

2.1. Materials

Additive manufacturing grade Ti alloy (Ti–6Al–4V; Grade 5) powder was directly purchased from EOS GmBH, Germany. The composition of Ti–6Al–4V powder is listed in Table 1.

2.2. Sample preparation

Additive manufacturing is a layer by layer manufacturing process to construct three dimensional (3D) objects from their corresponding metal powder. Here, selective laser melting (SLM) technique (EOS M290 model, Germany) was used to develop 3D objects from the design data. In this process, using CAD/CAM design software, various 3D models of solid as well as porous coupon samples with circular and square type pores were created. Subsequently, these 3D models were sliced into 2D layers. For printing of each layer, laser beam, scan speed, hatch space was chosen as per the EOS standard process parameters. As per the design data, the first layer of Ti–6Al–4V powder was spread over the bed; the laser beam selectively melted the powder and solidified it. Subsequently, the powder bed moved down and the fresh Ti–6Al–4V powder of similar layer thickness was again spread and labelled by a re-coater blade uniformly above the first printed layer. Again, the laser melting of the second layer takes place and will be solidified over the first layer. This powder spreading, melting and solidification process was repeatedly continued to build the final component. Once the printing process is done with, excess powder surrounding the component was sucked using a vacuum cleaner and the components were cut from the base plate using wire EDM to separate them for further studies. For printing the coupon type samples, porous support structure was also built as per the machine supplier protocol. During the complete printing process, the chamber was filled with argon gas to avoid the oxidation of Ti–6Al–4V powder as well as the printed component.

As a part of this study, scaffolds were heat-treated in the range of 1000–1300 °C in an argon gas atmosphere in a tubular furnace to determine the effect of temperature on sintering of loosely bonded Ti–6Al–4V particles found in the surrounding walls. A constant holding time of 2 h was maintained for every sample.

2.3. Surface modification of Ti–6Al–4V samples

Porous Ti–6Al–4V samples of size $10 \times 10 \times 10$ mm^3 were separately cleaned in an ultrasonic cleaner using acetone, isopropyl alcohol and ultrapure water for 15 min each. Thus prepared samples were then heated at 1300 °C for 1 h. These cubical samples were wire cut into $10 \times 10 \times 1$ mm^3 and cleaned as described above for surface modification

Table 1. Composition of Ti–6Al–4V powder used for the present study.

Powder composition	Wt. %
Al	5.5–6.5 %
V	3.5–4.5 %
O	<2000 ppm
N	<500 ppm
C	<800 ppm
H	<120 ppm
Fe	<2500 ppm
Ti	Balance

study. The heat treated samples were then chemically treated with 5 M NaOH (Sigma Aldrich, purity 98%) at 60 °C 120 rpm, 24 h. The NaOH treated samples were subsequently soaked in various concentrations of AgNO₃/Ca(NO₃)₂ (Sigma Aldrich, purity 99.8%) solutions at 40 °C, 120 rpm, 24 h. Finally, the unreacted chemicals were removed by a gentle wash with ultrapure water. In order to stabilise the surface modified layer, a heat treatment at 600 °C for 1 h was followed to all the chemically treated samples in an air atmosphere at a heating rate of 5 °C/min. The notations of the chemical and heat treatment conditions used in this work are listed in Table 2.

2.4. Evaluation of bioactivity in SBF

Samples listed in Table 2 were incubated in 30 ml of SBF and kept at 36.5 °C for 3 days. After the incubation time over, samples were collected from SBF, gently washed with ultrapure water and after gold sputtering their surfaces were observed under SEM [35].

2.5. Antibacterial study in S.aureus

The antibacterial properties of the samples listed in Table 2 were evaluated against gram positive bacteria *S.aureus* (MTCC, Chandigarh, India). Using the direct bacterial contact method, the antibacterial activity of these samples was evaluated. The sample surface was carefully covered with 100 μl of bacterial solution with a density of 10^6 CFU/ml, and was incubated at 37 °C for 6 h. After the incubation period was over, inoculated bacterial cell suspension was collected from the sample surfaces by force pipetting and making up to 1 ml in volume with fresh nutrient broth. The bacterial sample solution collected from each sample surface was used to prepare spread plates, which were then incubated at 37 °C. After 24 h, the colony formation was recorded for each sample conditions to examine the antibacterial activity.

2.6. Assessment of biocompatibility using osteoblast-like cells

The biocompatibility of SLMed porous Ti–6Al–4V samples after chemical and thermal treatments were evaluated using human osteoblast-like cells, MG63 (NCCS Pune, India), kept in Dulbecco's modified Eagle's medium (DMEM) using 10% fetal bovine serum (FBS) and 1% Penicillin–Streptomycin in a CO_2 incubator maintained at 37 °C and humidified atmosphere with 5% CO_2. Cells at 80–90% confluency were used in all experiments.

MTT assay was performed to determine whether SLMed porous Ti–6Al–4V samples treated with various chemical and thermal treatments exhibited cytotoxicity [28]. Samples of dimensions compatible to 96-well flat bottom tissue culture dish were cut, sterilized by autoclaving and placed in appropriate well under sterile condition. MG 63 cells at a density of 10,000 cells/well was seeded directly to the sample surface followed by fresh media added through the walls of 96-wells and cells without SLMed

samples served as the control. The plate with samples was incubated for 48 h in a CO_2 incubator. After the incubation period, the cell viability was examined using thiazolyl blue tetrazoliumbromide (Vybrant® MTT Cell Proliferation Assay Kit). The media was removed, and around 100 μl of MTT solution was added and then incubated for a period of 3 h, until the formation of formazan crystals. After 3 h, the insoluble formazan crystals were dissolved by adding dimethyl sulfoxide (DMSO) and the absorbance were read at 570 nm using an ELISA reader (CyberElisa-R01Automatic Micro-plate Reader, Cyberlab Corporation, USA) in triplicate.

For cell adhesion study, around 20,000 cells were seeded on each sample surface and incubated in a CO_2 incubator for 48 h. After the specified time period, the cells were fixed on the sample surfaces using 4% paraformaldehyde for 20 min, and nuclear staining was carried out. A confocal laser scanning microscope (CLSM; Carl Zeiss-LSM 880, Germany) was used to observe and record the morphology of MG63 cells adhered on the sample surface [28].

2.6.1. Statistics

All the datas were represented as mean ± standard error of the mean from n = 3 experiments and the statistical significance was considered using a Student's paired t-test (Sigmaplot) and represented as *: $P \leq 0.05$, **: $P \leq 0.01$, and ***: $P \leq 0.001$.

2.7. Characterisation of materials

The samples mentioned in Table 2 were further characterised using X ray Diffraction (XRD, Bruker, UK), Scanning Electron Microscope (SEM, TESCAN, Czech Republic), Laser Raman Spectroscopy (Horiba Jobin Yvon, LabRAM HR Evolution) of He–Ne laser with a wavelength of 532 nm.

3. Results and discussions

3.1. Powder characterization

The shape and size of the as-purchased Ti–6Al–4V powder were observed under SEM and the result is shown in Figure 1a. Spherical particles of Ti–6Al–4V with an average particle size of 45 μm can be observed from SEM images. The XRD pattern of Ti–6Al–4V powder (Figure 1b) shows the standard diffraction peaks at 36.1°, 38.9° and 40.3° 2θ values corresponding to α Ti metal. This powder was subsequently used for SLM as per the supplied EOS print parameters.

3.2. Preparation of porous Ti–6Al–4V alloy samples

To confirm the dimensional accuracy of the printed components, various types of pores were designed using design software and the printed sample photographs are shown in Figure 2a. Samples of pore dimensions varying from 0 to 1 mm were designed in a 10 × 10 × 10 mm³ cubical structure. The density, as well as the porosity of all the

Table 2. Notations for various chemical and heat treatments used in the present study.

| Chemical treatments	Notations
Untreated SLM built Ti –6Al–4V alloy heat treated at 1300 °C	3D-Ti64/Ti64
SLM built Ti –6Al–4V alloy heat treated at 1300 °C, treated with 5 M NaOH solutions, 60 °C, 24 h, heat treated at 600 °C, 1 h	3D- Ti64–Na–H/Ti64 –Na
SLM built Ti –6Al–4V alloy heat treated at 1300 °C, treated with 5 M NaOH solutions, 60 °C, 24 h and 0.01 mM AgNO₃ solution, 40 °C, 24 h, heat treated at 600 °C, 1 h	3D- Ti64–Na–Ag–H
SLM built Ti –6Al–4V alloy heat treated at 1300 °C, treated with 5 M NaOH solutions, 60 °C, 24 h and 100 mM Ca(NO₃)₂ solution, 40 °C, 24 h, heat treated at 600 °C, 1 h, heat treated at 600 °C, 1 h	3D- Ti64–Na–Ca–H
SLM built Ti –6Al–4V alloy heat treated at 1300 °C, treated with 5M NaOH solutions, 60 °C, 24 h and treated with a mixture of 1ml of 1 mM AgNO₃ & 9 ml of 100 mM Ca(NO₃)₂ solution, 40 °C, 24 h, heat treated at 600 °C, 1 h	3D- Ti64–Na–9Ca:1Ag–H/9Ca:1Ag
SLM built Ti –6Al–4V alloy heat treated at 1300 °C, treated with 5M NaOH solutions, 60 °C, 24 h and treated with a mixture of 0.5 ml of 1 mM AgNO₃ & 9.5 ml of 100 mM Ca(NO₃)₂ solution, 40 °C, 24 h, heat treated at 600 °C, 1 h.	3D- Ti64–Na-9.5Ca:0.5Ag–H/ 9.5Ca:0.5Ag
SLM built Ti –6Al–4V alloy heat treated at 1300 °C, treated with 5M NaOH solutions, 60 °C, 24 h and treated with a mixture of 0.1 ml of 1 mM AgNO₃ & 9.9 ml of 100 mM Ca(NO₃)₂ solution, 40 °C, 24 h, heat treated at 600 °C, 1 h.	3D- Ti64–Na-9.9Ca:0.1Ag–H/ 9.9Ca:0.1Ag
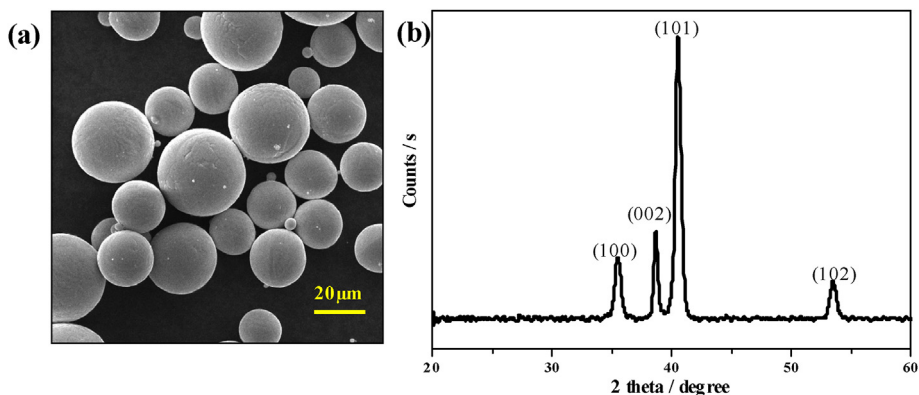
Figure 1. (a) SEM image of as-purchased Ti–6Al–4V powder used for the study. Powder morphology appeared to be spherical with a range of particle size. (b) XRD spectra of Ti–6Al–4V powder shows peaks corresponding to pure Ti metal.
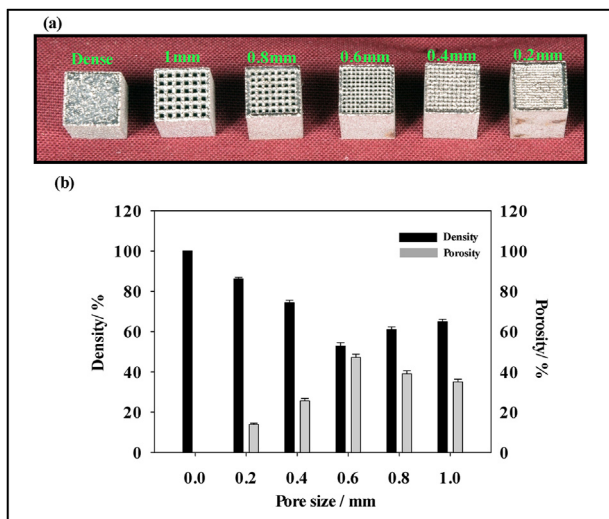

Figure 2. (a) Photographs of SLM Ti–6Al–4V cubical samples with varying pore dimensions from 200 to 1000 μm. For comparison dense sample image is also shown. (b) Graphical representation of density/porosity Vs pore size as measured by Archimedes principle.

Ti–6Al–4V cubical samples, was measured by Archimedes principle as shown in Eq. (1) and the results are shown in Figure 2b.

$$\text{Density of the sample} = Wa \,/\, (Wa - Ww) \qquad (1)$$

Where, Wa = Weight of sample in air & Ww = Weight of sample in water.

Percentage of porosity was calculated from the density of the samples while the theoretical density of Ti–6Al–4V powder was taken as 4.41 g/cc. The solid cubical Ti–6Al–4V sample developed by the SLM technology showed a density ˃99.5% and samples containing pores with 200 μm in size reduced the density to 85–90%. Around 50–60% density was observed for samples with a pore dimension of 600 μm and above and it can be controlled by controlling the number of continuous pores in a fixed sample dimension. This study clearly shows that under defined process parameters, uniform pores with good dimensional accuracy could be designed and developed. More interestingly, from visual observation, pore size of 200 μm and above showed continuous and uniform porosity. It is clearly evident that the bone implant scaffold of such pore size and above could be easily fabricated by the present SLM technique.

Many researchers have investigated various design parameters which give faster bone integration and growth at bone defects. Karageorgiou et al., observed that lower porosity in implants leads to osteogenesis *in vitro* whereas greater bone ingrowth was observed with higher porosity and pore size. However, the mechanical properties of the implant diminish here. A minimum requirement for pore size is 100 μm and a

pore size greater than 300 μm enhances the bone and capillary formation [4]. Harvey et al., reported that 45% porosity with a pore size of 350μm can reduce the stress-related bone resorption in implants [36]. Another study by Chang et al., showed a maximum bone ingrowth at porosity in the range of 50–60% and a pore size of 170 μm [37]. Bobyn et al., reported that maximum bone ingrowth and fixation was observed at implants with 50–400 μm pore size [38]. Fukuda et al., studied the effect of different pore sizes ranging from 500-1200 μm on the osteoinduction in Ti implants and observed a significant osteoinduction in the Ti implants having pore sizes in the range of 500–600 μm [39]. In contrast to these reports, Itala et al., reported that the bone ingrowths in the implant are independent of the pore size or its thickness [40]. Along with pore size and porosity, bone ingrowth or new bone formation on an implant greatly depends on the interconnectivity of pores. Yoshikawa et al. reported that implants with interconnected pores showed good osteo-conduction [41]. Otsuki et al. used the help of micro CT scan to determine the effect of interconnectivity on the bone ingrowth and concluded that well-differentiated pore throats have more tissue ingrowth than that in the narrow pore throats [42].

3.3. Heat treatment studies

As evident from the image of the as-printed sample, a significant amount of un-melted Ti–6Al–4V particles were adhering on the inner walls of the SLM printed porous structure. The un-melted particles may detach and get released into the human body leading to health issues. Therefore, it is essential to carry out post-treatment either to bond these loose particles or remove them from the porous walls. A simple heat treatment study was carried out in the range of 1000 to 1300 °C in an inert atmosphere to inspect the powder sintering possibilities. Figure 3 shows the SEM images of Ti–6Al–4V printed samples heat-treated at different temperatures. At 1200 °C, the loosely bonded metal particles were found to be sintered with each other as well as onto the walls of the porous structure. SEM image of sample heat-treated at 1300 °C clearly shows the occurrence of the particle to particle sintering, with neck formation. During the heat treatment process, micro-pockets were also found to have formed throughout the sample due to metallic particle diffusion as well as sintering, by which an increase in the anchorage of surrounding bone tissues via ingrowths of bone minerals is anticipated. Based on the above study, an optimum temperature for the heat treatment could be chosen in the range of 1200 °C to 1300 °C. It is well understood that heat treatment also affects the mechanical properties as well as the microstructures of the components and therefore requires further investigation [39, 43, 44]. Porous Ti–6Al–4V samples heated at 1300 °C were used for further studies to improve the bioactivity for better osteointegration.

Even though macroporosity can provide good osteogenesis, micro porosity/surface roughness plays a major role in bringing protein
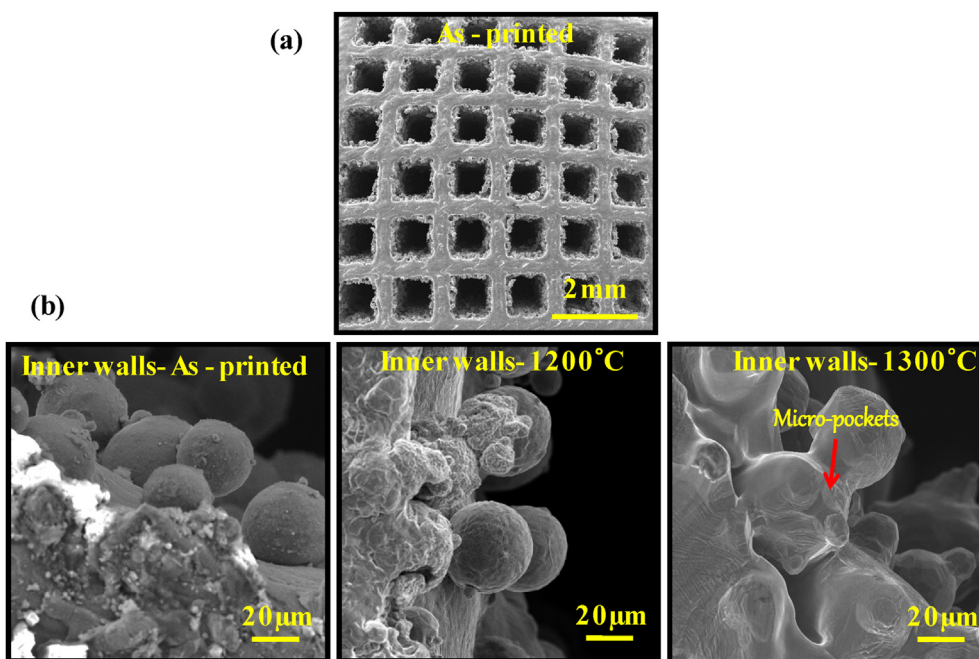
Figure 3. (a) SEM images of a typical SLM built Ti–6Al–4V samples with square shaped pores. (b) SEM images of inner walls of as-printed porous Ti–6Al–4V sample and heat treated at 1200 and 1300 °C. As-printed samples showed weakly bonded Ti–6Al–4V particles even up to 1200 °C and these particles became soften when sintered above 1300 °C and finally bonded to the walls of the components leading to micro-pockets.

adsorption, cell adhesion, bone-like apatite formation etc. in implants. To improve the bioactivity as well as bone integration of Ti alloys, surface modification by chemical treatment methods are most appropriate as it results in uniform application in both inner and outer walls of complicated porous structures.

3.4. Surface modification of Ti–6Al–4V samples

SEM images of porous Ti–6Al–4V samples, treated with NaOH and NaOH–Ca(NO₃)₂/AgNO₃ solution followed by heat treatment at 600 °C are shown in Figure 4. The SEM images of the samples before

subjecting to NaOH and heat treatment is also shown for comparison (Figure 4a). The SEM images of samples heat-treated at 1300 °C clearly show a smooth uniform surface which gets transformed into a highly porous network-like structure by the subsequent NaOH solution treatment and thus formed porous network did not get affected by the subsequent heat treatment. From the SEM images, it could be noticed that even the inner walls of the samples formed porous network-like structures. This indicates that the NaOH treatment method followed here has the advantages of uniform chemical treatment including the inner walls of the porous samples which could not be achieved through other methods.
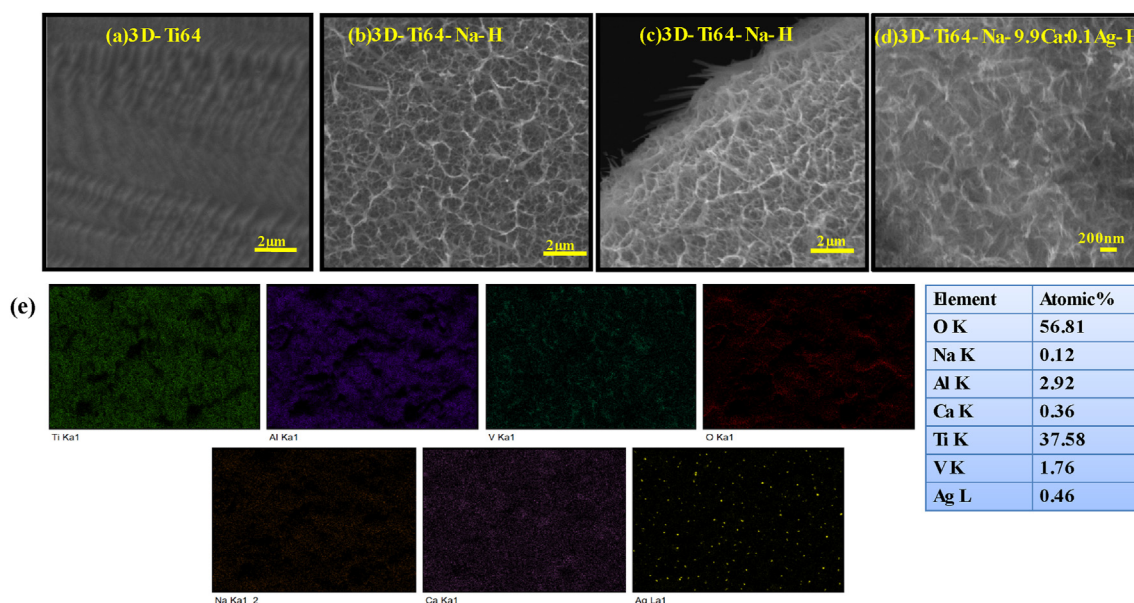

Figure 4. SEM images of porous Ti–6Al–4V samples (a) heat treated at 1300 °C, (b) & (c) subjected to subsequent soaking in NaOH solution and further heat treatment at 600 °C. NaOH treatment showed the formation of fine porous network structure both walls as well as melted particles inside the pores confirming the uniform chemical tretatment.(d) & (e) SEM image & EDS result of porous Ti–6Al–4V samples, heat treated at 1300 °C, subjected to NaOH and subsequently treated with a mixture of Ca and Ag nitrate solutions and heat treatment at 600 °C.
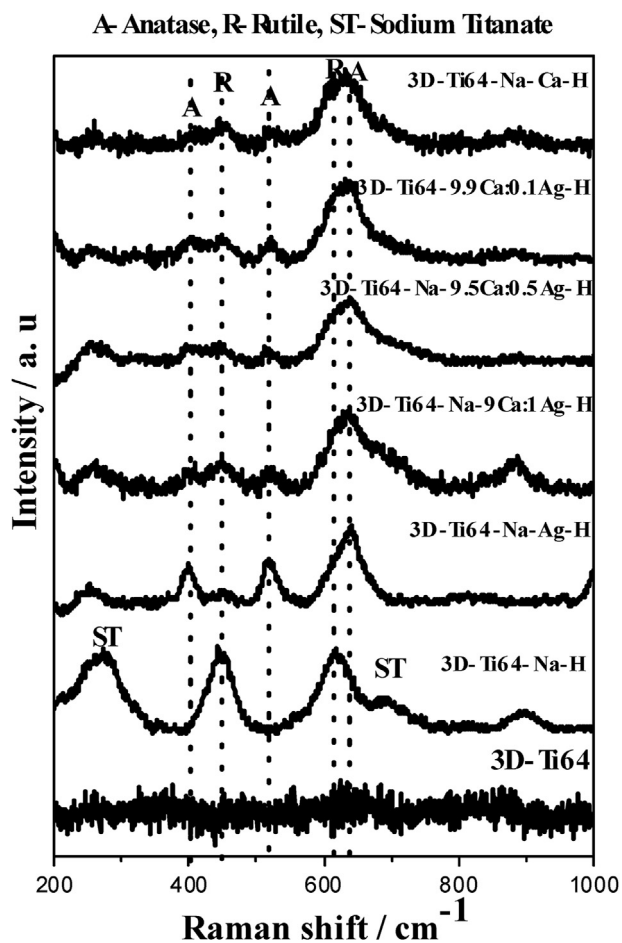
Figure 5. Raman spectra of porous Ti–6Al–4V samples heat treated at 1300 °C, subjected to various chemical and heat treatments.

The NaOH treated Ti–6Al–4V sample was subsequently treated with a mixture of Ca and $AgNO_3$ solution, to replace the Na^+ ions with Ca^{2+}/Ag ions. Figure 4d shows the SEM images of porous Ti–6Al–4V samples after NaOH and subsequently treated with a mixture of Ca and Ag nitrate solutions, heat-treated at 600 °C. It could be observed from the SEM image, that the morphology of alkali-Ca/Ag- heat-treated surface is similar to that of only alkali and heat-treated surface. The EDS analysis was carried out to measure the surface elemental composition present on the chemically treated samples and the result shows the presence of Ca and Ag in addition to Ti, O, Al, V and a trace amount of Na. Around 0.36 at % of Ca and 0.46 at % Ag was decorated over the sample surface when treated with 9.5 ml of 100 mM $Ca(NO_3)_2$ and 0.5 ml of 1 mM $AgNO_3$ solution. The concentration of $Ca(NO_3)_2$ and $AgNO_3$ solution was chosen based on the optimised results attained by the author earlier [28, 33].

The phases formed on porous Ti–6Al–4V samples listed in Table 2 were studied by Laser Raman spectroscopy and the result is shown in Figure 5. As seen from the Raman spectra, the sample heat treated at 1300 °C in an inert atmosphere showed a straight line which indicates no oxide layer formation over the SLMed Ti–6Al–4V. Peaks corresponding to sodium titanate as well as rutile TiO_2 were observed when the Ti–6Al–4V sample was subjected to NaOH and heat treatment. When the Na^+ ions were exchanged with Ag^+ ions during $AgNO_3$ treatment, the sodium titanate and rutile TiO_2 peaks disappeared and peaks corresponding to anatase TiO_2 appeared. When the NaOH treated Ti–6Al–4V samples were treated with a mixture of Ca–Ag solution and heat treatment, peaks corresponding to both anatase as well as rutile TiO_2 were observed. The anatase to rutile TiO_2 formation was observed to be increasing with an increase in silver ratio. The NaOH–Ca-heat sample showed peaks corresponding to rutile TiO_2 along with a trace amount of anatase TiO_2. The chemically and heat treated SLMed Ti–6Al–4V samples were further soaked in SBF to evaluate its *in vitro* bioactivity (apatite forming ability).

3.5. Preliminary evaluation of bioactivity in SBF

Figure 6a & b shows that SLMed Ti–6Al–4V samples subjected to NaOH and heat treatment as well as NaOH–Ag and heat treatment when incubated in SBF showed bone-like apatite formation on its surface whereas NaOH–Ca-heat did not. Surprisingly, porous Ti–6Al–4V samples
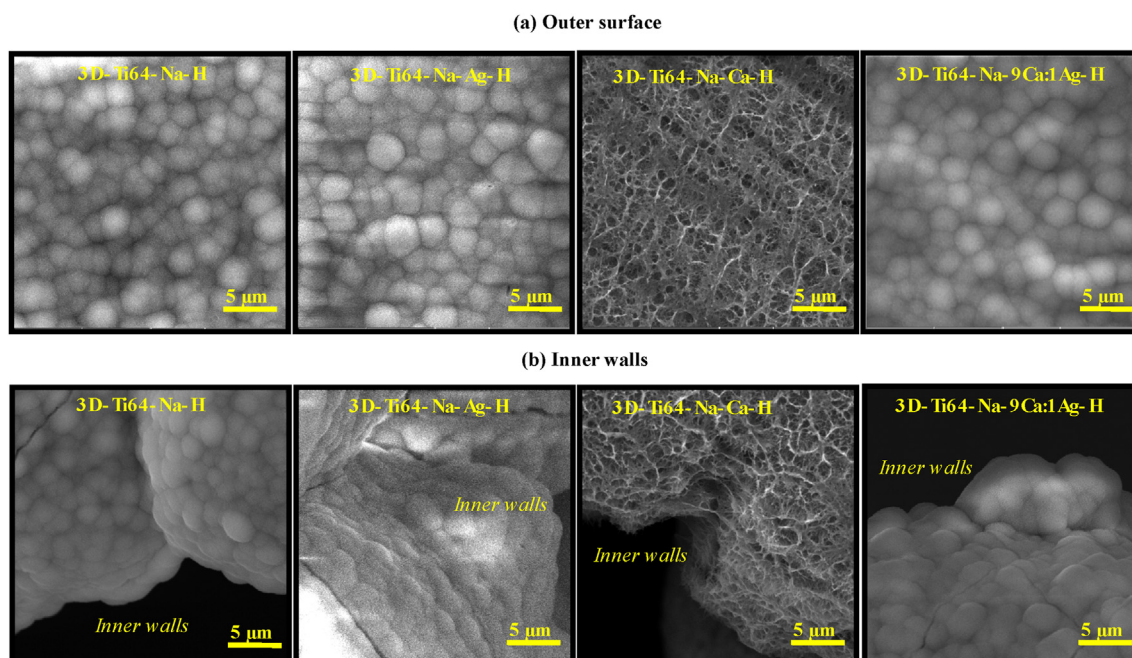
(a) Outer surface

(b) Inner walls

Figure 6. (a) & (b) SEM images of porous Ti–6Al–4V samples, subjected to various chemical and heat treatments and soaked in SBF for 3 days, and observed at outer surface as well as inside the pores. Bone-like apatite particles could be observed even in the inner walls of chemical and heat treated samples.

subjected NaOH–Ca/Ag-heat (co-doped) formed bone-like apatite. This increased apatite formation could be attributed to the formation of anatase TiO_2 as indicated in Figure 5 [27].

Ti metal and its alloys when treated with NaOH form a network-like morphology of 1 μm thickness which gets converted to a bioactive sodium titanate upon heat treatment at 600 °C [20, 21, 22, 23]. In SBF, these Na^+ ions release from the alkali-treated Ti metal/Ti alloy into the surrounding fluid, making a surface negative charge. This in turn attracts more amounts of Ca^{2+} ions followed by PO_4^{3-} ions from the surrounding SBF forming bone-like apatite on its surface. Similar results were also observed in the present study. The cytotoxic effects caused by thus released Na^+ are a serious concern when it comes to the real application. Therefore, in the present study, these Na^+ ions have been replaced by Ca^{2+}/Ag^+ ions to provide a "Na-free" surface with an expectation of additional advantages for properties such as osteoblastic cell compatibility and antibacterial activity, respectively. However, when it comes to the bone-like apatite formation in SBF, Ca or Ag or Ca–Ag co-decorated Ti–6Al–4V alloy surfaces behave differently. As we could see from Figure 6, only Ag decorated Ti–6Al–4V alloy formed bone-like apatite whereas only Ca containing surface did not. Surprisingly, when Ca and Ag were co-decorated on the Ti–6Al–4V alloy surface, the bone-like apatite formation could be retained on its surface. From our previous studies and also from the present results, it can be seen that only Ag decorated surface formed anatase TiO_2 whereas rutile TiO_2 was dominant in the case of only Ca decorated Ti–6Al–4V alloy surface [32, 33]. When it comes to the co-decoration of Ca and Ag, anatase TiO_2 peaks became more prominent. The formation of anatase TiO_2 in the case of only Ag and Ca–Ag co-decorated Ti–6Al–4V alloy could be a reason which triggered bone-like apatite formation in this case. Although Ca–Ag co-doped macro-micro-nano porous network structure developed over Ti–6Al–4V sample induces bioactivity in SBF, the amount of Ag incorporated should exhibit antimicrobial activity. Therefore, further studies on the antibacterial efficiency of the Ca–Ag treated porous Ti–6Al–4V surfaces were carried out using *S. aureus* bacteria.

3.6. Antibacterial study

The Ca–Ag volume ratio optimised from the previous studies (9.9Ca:0.1Ag) were used here and compared with that of alkali-heat treated porous Ti–6Al–4V samples [28, 33, 34]. Figure 7 (a-b) shows the results of the antibacterial study carried out for the samples subjected to chemical and heat treatments. Direct contact method was followed to evaluate the antibacterial activity of the above surfaces. As we could see from the photographs of spread plates prepared from the cells incubated with the respective samples, porous Ti–6Al–4V samples treated with NaOH and heat showed a similar number of *S. aureus* colonies whereas no bacterial colonies could be observed in the porous Ti–6Al–4V samples, treated with NaOH–Ca/Ag and heat treatment. A minimum Ca:Ag ratio of 9.9:0.1 was found to be good enough for the complete killing of *S.aureus* cells (Figure 7a). In order to obtain a quantitative analysis of the antibacterial study, experiment was done in triplicate for the chemical and heat treatment conditions and the statistical analysis of the result is shown in Figure 7b.

3.7. MTT assay and cell adhesion study

A quantitative analysis on the biocompatibility of SLMed porous Ti-6Al–4V samples subjected to various chemical and thermal treatments was carried out using MTT assay and is presented in Figure 8a. As we could observe from the figure, the viability of the cells grown along with the samples was more or less similar to that in the control cells grown in the absence of samples. This in turns indicates that all the samples, irrespective of the chemical composition, is biocompatible and the incorporated Ag ions in all the 3 ratios, 9:1, 9.5:0.5 and 9.9:0.1, are not
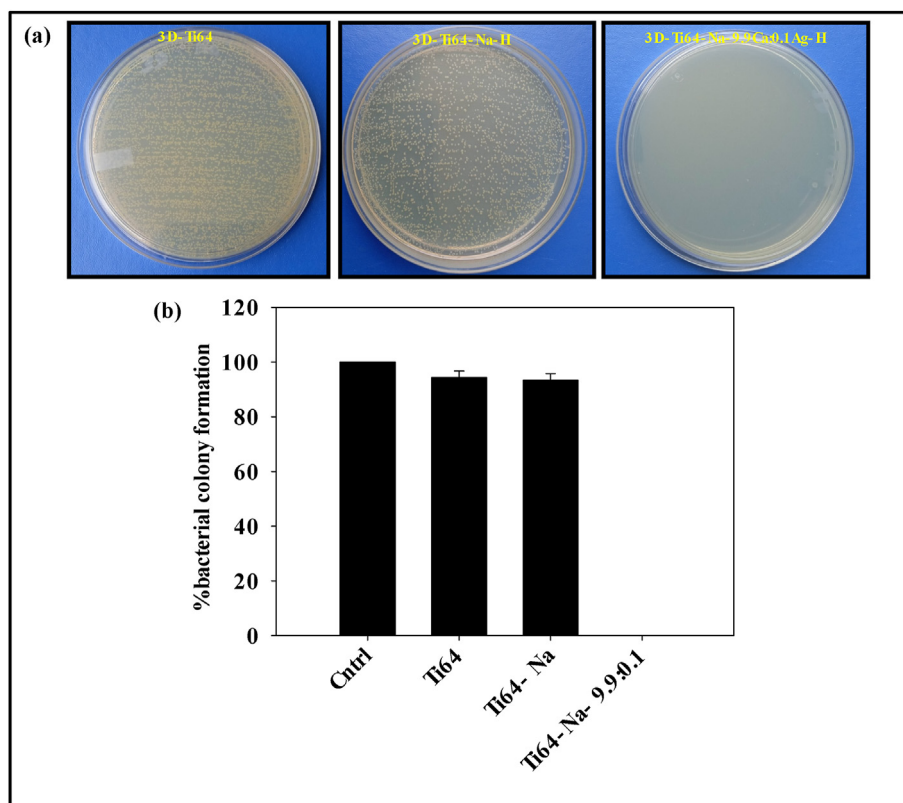

Figure 7. (a) Antibacterial study carried out for porous Ti–6Al–4V samples, subjected to various chemical and heat treatments. Untreated Ti–6Al–4V as well as NaOH and heat-treated sample did not show any antibacterial activity (presence of bacterial colonies) while Ca–Ag decorated Ti–6Al–4V showed good antibacterial activity (no bacterial colonies). (b) Quantitative analysis of antibacterial activity for the samples measured as % bacterial colony formation.
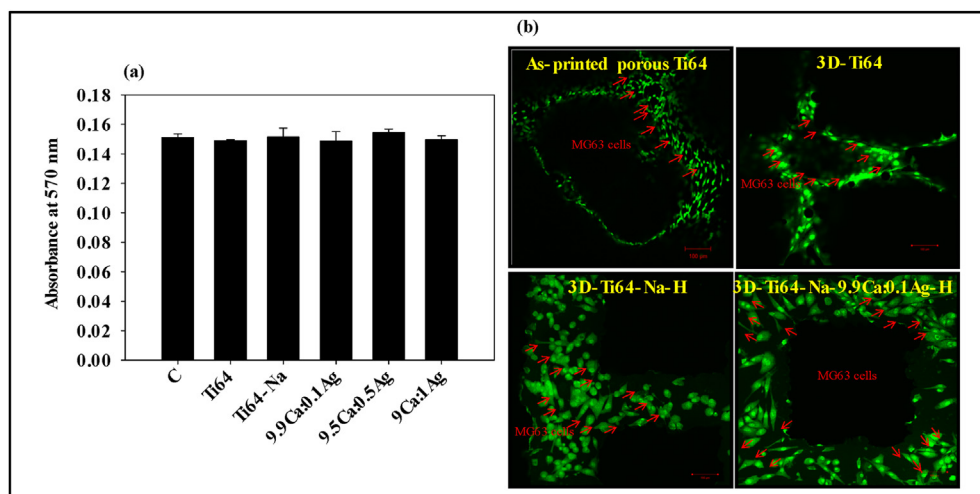
Figure 8. (a) Cell viability of SLM built porous Ti–6Al–4V samples subjected to various chemical and thermal treatments as measured by MTT assay. (b) CLSM images of MG 63 cells adhered on as-printed Ti–6Al–4V samples, SLM built porous Ti–6Al–4V samples sintered at 1300 °C subjected to various optimized chemical and heat treatments, after acridine orange staining. Significant amount of MG 63 cells adherence on Ca–Ag sample indicates the non-toxicity of the Ag concentration present on the Ti–6Al–4V sample surface.

toxic to the cells. In order to study the adhesion and spreading property of MG63 cells on SLMed Ti–6Al–4V samples incorporated with Ag/Ca ions, the samples were seeded with cells and were incubated for a period of 48 h. After the incubation period, these samples were collected, washed and the cells adhered on the sample surfaces were fixed using para-formaldehyde and stained using acridine orange. Later, the samples were observed under CLSM and the images of the cells adhered on the surfaces were captured at different locations of the porous structure. Figure 8b shows the CSLM images of MG 63 cells adhered on the walls of the as-printed porous Ti–6Al–4V sample, porous Ti–6Al–4V samples heat treated at 1300 °C, subjected to various chemical and heat treatments. From the images, it can be concluded that the cells observed were alive and healthy over the Ti–6Al–4V samples for 48 h. The morphology of the cells appeared to be intact which further indicates that the sample is non-toxic to the bone cells. However, for better bone integration, surface modification approaches needs to be adopted in the SLMed Ti–6Al–4V components and their osteoblastic cell compatibility to be evaluated on MG 63 cells. All the samples, irrespective of the chemical treatment, showed good osteoblastic cell compatibility towards MG 63 cells and the cell morphology was also observed to be intact and healthy. The minimum Ca:Ag ratio of 9.9:0.1 which showed complete killing efficiency towards *S. aureus*, also showed good osteoblastic cell compatibility towards MG 63 cells.

Based on the overall study, it can be summarised that the AM technologies as described here and also reported by several researchers have their advantages of design and development of PSI mimicking to the damaged or diseased patient bones. This technology can even help to mimic the porosity, patient bone density, bone structures, etc. making it superior to any other conventional implant manufacturing method. Continuous pores of size 200 μm and above could be fabricated by the SLM technology. Although PSIs are developed, modification of implant surface by chemical treatment is required for better bone integration. The present study showed a cost-effective, easy method by co-doping the Ca–Ag ions that promoted faster bioactivity as well as antibacterial activity. The antibacterial treatment presented here has a unique advantage of preventing implant-related infections, implant rejection and secondary surgery which is not a desirable case for any patient. Macro-/micro-nanoporosity over SLM built Ti–6Al–4V alloy surface from its powder proposed in the study is a novel idea that can improve the tissue ingrowth and tight implant fixation in the case of permanent PSI's such as hip, knee, dental screw, spine spacers, etc. Although the present study proved better bioactivity, antibacterial activity and osteoblastic cell compatibility, the bone integration studies in animal models needs to be carried out to confirm the faster osteointegration to establish that the chemical followed by thermal treatment method is highly useful and effective for developing hard tissue replacement implants.

4. Conclusions

- Selective laser melting technique was found to be useful to develop Ti–6Al–4V scaffold from its corresponding alloy powder with channel type macro-micro porous structure. Pore size of 200 μm and above with high degree of dimensional accuracy could be successfully printed using this SLM technology.
- Loosely bonded particle adhering to the inner and outer walls of the porous structure could be fused and bonded by the subsequent heat treatment at 1300 °C to form not only micro pockets for tissue ingrowth and also avoid the release of metal particles during its use.
- The surface modification method using NaOH treatment formed a fine nanoporous network structure over the Ti–6Al–4V porous sample where Ca or Ag or Ca–Ag ions could be subsequently decorated by replacing the Na ions.
- Raman results showed only Ca containing samples has rutile phase while only Ag or Ca–Ag co-decoration lead to anatase TiO_2 phase over Ti–6Al–4V porous samples.
- *In vitro* bioactivity result in simulated body fluid showed Ag and Ca–Ag co-decorated samples accelerated the apatite deposition in contrast to only Ca incorporated samples possibly due to the formation of anatase TiO_2 phase in former conditions.
- Ca–Ag co-decorated nano porous network surface over Ti–6Al–4V alloy scaffolds lead to the formation of bioactive, antibacterial and cell compatible surface which will be very useful in the biomedical field while developing patient specific implants.

Declarations

Author contribution statement

Archana Rajendran: Conceived and designed the experiments; Performed the experiments; Analyzed and interpreted the data; Wrote the manuscript.

Deepak K. Pattanayak: Conceived and designed the experiments; Analyzed and interpreted the data; Corrected the manuscript.

Data availability statement

Data will be made available on request.

References

[1] L.L. Hench, Bioceramics: from concept to clinic, J. Am. Ceram. Soc. 74 (1991) 1487–1510.

[2] D. Williams, X. Zhang, Definitions of Biomaterials for the Twenty-First Century, 1st ed, Elsevier, 2019.

[3] S. Gross, E.W. Abel, A finite element analysis of hollow stemmed hip prostheses as a means of reducing stress shielding of the femur, J. Biomech. 34 (2001) 995–1003.

[4] V. Karageorgiou, D. Kaplan, Porosity of 3 D biomaterial scaffolds and osteogenesis, Biomaterials 26 (2005) 5474–5491.

[5] C.W. Kang, F.Z. Fang, State of the art of bioimplants manufacturing: part I, Adv. Manuf. 6 (2018) 20–40.

[6] M. Tilton, G.S. Lewis, G.P. Manogharan, Additive manufacturing of orthopedic implants, in: B. Li, T. Webster (Eds.), Springer International Publishing AG, Part of Springer Nature, Orthopedic Biomaterials, 2018.

[7] G. Ryan, A. Pandit, D.P. Apatsidis, Fabrication methods of porous metals for use in orthopaedic applications, Biomaterials 27 (2006) 2651–2670.

[8] D.K. Pattanayak, T. Matsushita, H. Takadama, A. Fukuda, M. Takemoto, S. Fujibayashi, K. Sasaki, N. Nishida, T. Nakamura, T. Kokubo, Fabrication of bioactive porous Ti metal with structure similar to human cancellous bone by selective laser melting, Bioceram. Dev. Appl. 1 (2011) 1–3.

[9] D.K. Pattanayak, A. Fukuda, T. Matsushita, M. Takemoto, S. Fujibayashi, K. Sasaki, N. Nishida, T. Nakamura, T. Kokubo, Bioactive Ti metal analogous to human cancellous bone: fabrication by selective laser melting and chemical treatments, Acta Biomater. 7 (2011) 1398–1406.

[10] X. Liu, P.K. Chu, C. Ding, Surface modification of titanium, titanium alloys, and related materials for biomedical applications, Mater. Sci. Eng. R 47 (2004) 49–121.

[11] T. Kokubo, F. Miyaji, H.M. Kim, T. Nakamura, Preparation of bioactive Ti and its alloy via simple chemical surface treatment, J. Biomed. Mater. Res. 32 (1996) 409–417.

[12] B.H. Lee, Y.D. Kim, J.H. Shin, K.H. Lee, Surface modification by alkali and heat treatments in titanium alloys, J. Biomed. Mater. Res. 61 (2002) 466–473.

[13] T. Kokubo, D.K. Pattanayak, S. Yamaguchi, H. Takadama, T. Matsushita, T. Kawai, M. Takemoto, S. Fujibayashi, T. Nakamura, Positively charged bioactive Ti metal prepared by simple chemical and heat treatments, J. R. Soc. Interface 7 (2010). S503–S513.

[14] J. Rieu, A. Pichat, L.M. Rabbe, A. Rambert, C. Chabrol, M. Robelet, Ion implantation effects on friction and wear of joint prosthesis materials, Biomaterials 12 (1991) 139.

[15] R.A. Buchanan, E.D. Rigney Jr., J.M. Williams, Wear-accelerated corrosion of Ti-6Al-4V and nitrogen-ion-implanted Ti-6Al-4V: mechanisms and influence of fixed-stress magnitude, J. Biomed. Mater. Res. 21 (1987) 367.

[16] A. Trampuz, A.F. Widmer, Infections associated with orthopedic implants, Curr. Opin. Infect. Dis. 19 (2006) 349–356.

[17] Z. Jia, P. Xiu, P. Xiong, W. Zhou, Y. Cheng, S. Wei, Y. Zheng, T. Xi, H. Cai, Z. Liu, C. Wang, W. Zhang, Z. Li, Additively manufactured macroporous titanium with silver releasing micro-/nanoporous surface for multipurpose infection control and bone repair − A proof of concept, ACS Appl. Mater. Interfaces 8 (2016), 28495–28510.

[18] A. Trampuz, W. Zimmerli, Antimicrobial agents in orthopaedic surgery: prophylaxis and treatment, Drugs 66 (2006) 1089–1105.

[19] B. Reidy, A. Haase, A. Luch, A.D. Kenneth, I. Lynch, Mechanisms of silver nanoparticle release, transformation and toxicity: a critical review of current knowledge and recommendations for future studies and applications, Materials 6 (2013) 2295–2350.

[20] H.M. Kim, F. Miyaji, T. Kokubo, T. Nakamura, Preparation of bioactive Ti and its alloys via simple chemical surface treatment, J. Biomed. Mater. Res. 32 (1996) 409–417.

[21] W.A. Camargo, S. Takemoto, J.W. Hoekstra, S.C.G. Leeuwenburgh, J.A. Jansen, J.J.J.P. Beucken, H.S. Alghamdi, Effect of surface alkali-based treatment of titanium implants on ability to promote in vitro mineralization and in vivo bone formation, Acta Biomater. 57 (2017) 511–523.

[22] K. Gulati, Ho-J Moon, T. Li, P.T. Sudheesh Kumar, S. Ivanovski, Titania nanopores with dual micro-/nano-topography for selective cellular bioactivity, J. Mater. Sci. Eng. C 91 (2018) 624–630.

[23] T. Kokubo, S. Yamaguchi, Bioactive titanate layers formed on titanium and its alloys by simple chemical and heat treatments, Open Biomed. Eng. J. 9 (2015) 29–41.

[24] D.K. Pattanayak, S. Yamaguchi, T. Matsushita, T. Kokubo, Nanostructured positively charged bioactive TiO_2 layer formed on Ti metal by NaOH, acid and heat treatments, J. Mater. Sci. Mater. Med. 22 (2011) 1803–1812.

[25] T. Kokubo, D.K. Pattanayak, S. Yamaguchi, H. Takadama, T. Matsushita, T. Kawai, M. Takemoto, S. Fujibayashi, T. Nakamura, Positively charged bioactive Ti metal prepared by simple chemical and heat treatments, J. R. Soc. Interface 96 (2010) S503–S513.

[26] Y. Yao, S. Liu, M.V. Swain, X. Zhang, K. Zhao, Y. Jian, Effects of acid-alkali treatment on bioactivity and osteoinduction of porous titanium: an in vitro study, J. Mater. Sci. Eng. C 94 (2019) 200–210.

[27] M. Nesabi, A. Valanezhad, S. Safaee, T. Odatsu, S. Abe, I. Watanabe, A novel multi-structural reinforced treatment on Ti implant utilizing a combination of alkali solution and bioactive glass sol, J. Mech. Behav. Biomed. Mater. 124 (2021) 104837.

[28] A. Rajendran, G. Vinoth, J. Nivedhitha, K.M. Iyer, D.K. Pattanayak, Ca-Ag coexisting nano-structured titania layer on Ti metal surface with enhanced bioactivity, antibacterial and cell compatibility, J. Mater. Sci. Eng. C 99 (2019) 440–449.

[29] D. Chopra, K. Gulati, S. Ivanovski, Understanding and optimizing the antibacterial functions of anodized nano-engineered titanium implants, Acta Biomater. 127 (2021) 80–101.

[30] H. Chouirfa, H. Bouloussa, V. Migonney, C. Falentin-Daudré, Review of titanium surface modification techniques and coatings for antibacterial applications, Acta Biomater. 83 (2019) 37–54.

[31] S. Nishiguchi, S. Fujibayashi, H.M. Kim, T. Kokubo, T. Nakamura, Biology of alkali- and heat-treated titanium implants, J. Biomed. Mater. Res. A. 67 (2003) 26–35.

[32] A. Rajendran, U. Kapoor, J. Nivedhitha, N. Lenka, D.K. Pattanayak, Effect of silver-containing titania layers for bioactivity, antibacterial activity, and osteogenic differentiation of human mesenchymal stem cells on Ti metal, ACS Appl. Bio Mater. 2 (2019) 3808–3819.

[33] A. Rajendran, S. Sugunapriyadharshini, D. Mishra, D.K. Pattanayak, Role of calcium ions in defining the bioactivity of surface modified Ti metal, J. Mater. Sci. Eng. C 98 (2019) 197–203.

[34] S. Spriano, S. Yamaguchi, F. Baino, S. Ferraris, A critical review of multifunctional titanium surfaces: new frontiers for improving osseointegration and host response, avoiding bacteria contamination, Acta Biomater. 79 (2018) 1–22.

[35] T. Kokubo, H. Takadama, How useful is SBF in predicting in vivo bone bioactivity? Biomaterials 27 (2006) 2907–2915.

[36] E.J. Harvey, J.D. Bobyn, M. Tanzer, G.J. Stackpool, J.J. Krygier, S.A. Hacking, Effect of flexibility of the femoral stem on bone remodeling and fixation of the stem in a canine total hip arthroplasty model without cement, J Bone Joint Surg. Am. 81 (1999) 93–107.

[37] Y.S. Chang, H.O. Gu, M. Kobayashi, M. Oka, Influence of various structure treatments on histological fixation of titanium implants, J. Arthroplasty 13 (1998) 816–825.

[38] J.D. Bobyn, R.M. Pilliar, H.U. Cameron, G.C. Weatherly, The optimum pore size for the fixation of porous-surfaced metal implants by the ingrowth of bone, Clin. Orthop. Relat. Res. 150 (1980) 263–270.

[39] A. Fukuda, M. Takemoto, T. Saito, S. Fujibayashi, M. Neo, D.K. Pattanayak, T. Matsushita, K. Sasaki, N. Nishida, T. Kokubo, T. Nakamura, Osteoinduction of porous Ti implants with a channel structure fabricated by selective laser melting, Acta Biomater. 7 (2011) 2327–2336.

[40] A.I. Itala, H.O. Ylanen, C. Ekholm, K.H. Karlsson, H.T. Aro, Pore diameter of more than 100 micron is not requisite for bone ingrowth in rabbits, J. Biomed. Mater. Res. 58 (2001) 679–683.

[41] H. Yoshikawa, N. Tamai, T. Murase, A. Myoui, Interconnected porous hydroxyapatite ceramics for bone tissue engineering, J. R. Soc. Interface 6 (2009). S341–S348.

[42] B. Otsuki, M. Takemoto, S. Fujibayashi, M. Neo, T. Kokubo, T. Nakamura, Pore throat size and connectivity determine bone and tissue ingrowth into porous implants: three-dimensional micro-CT based structural analyses of porous bioactive titanium implants, Biomaterials 27 (2006) 5892–5900.

[43] L. Huang, B. Cai, Y. Huang, J. Wang, C. Zhu, K. Shi, Y. Song, G. Feng, L. Liu, L. Zhang, Comparative study on 3D printed Ti6Al4V scaffolds with surface modifications using hydrothermal treatment and microarc oxidation to enhance osteogenic activity, ACS Omega 6 (2021) 1465–1476.

[44] D.P. Ming, S. Shao, J. Qiu, J. Yang, Y. Yu, J. Chen, W. Zhu, C. Tang, Superiority of calcium-containing nanowires modified titanium surface compared with SLA titanium surface in biological behavior of osteoblasts: a pilot study, Appl. Surf. Sci. 416 (2017) 790–797.